UFSM

CIÊNCIA e NATURA

ISSN 2179-460X
OPEN ACCESS

Ci. e Nat., Santa Maria, e86389, v. 47, 2025 • https://doi.org/10.5902/2179460X86389
Submitted: 12/01/2024 • Approved: 18/02/2025 • Published: 01/04/2025

Chemistry

Chitosan/smectite spheres for methylene blue removal: preparation and characterization

Esferas de quitosana/esmectita para remoção de azul de metileno: preparação e caracterização

Mateus Veras Pereira[I], Mauro Cosme de Carvalho Goes[II], Rodolfo Araújo Fernandes[II], Suzyeth Monteiro Melo[II], Joacy Batista de Lima[II], Cicero Wellington Brito Bezerra[II]

[I] Universidade Estadual de Campinas, Campinas, SP, Brasil
[II] Universidade Federal do Maranhão, Departament of Chemistry, São Luís, MA, Brasil

ABSTRACT

Effluent treatment and water body decontamination are pressing global challenges due to high water consumption and industrial effluent generation. This study focused on developing efficient, cost-effective adsorbents for the removal of methylene blue, a widely used dye known for its toxicity. Chitosan (CS) and smectite clay composites were prepared and characterized using FTIR, XRD, and pHpzc analyses. FTIR confirmed the preservation of the functional groups of both materials in the prepared composite, whereas the diffractograms indicated a superficial interaction, as evidenced by the absence of shifts in the diffractogram peaks. The point of zero charge pH on the surface of the CS/Clay-180 and CS/Clay-580 composites was evaluated as 8.5 and 8.4, respectively. Adsorption experiments covered a pH range of 3 - 11, exposure times of up to 600 min and dye concentrations from 5 - 350 mg L^{-1}. Kinetic data followed first and second-order models, while the Freundlich model best described the experimental isotherms. Our composites exhibited excellent adsorption capacities, with maximum values of 45.4 mg g^{-1} for CS/Clay-180 and 42.7 mg g^{-1} for CS/Clay-580, at pH 10 and a contact time of 300 min. Therefore, the prepared CS/clay spheres proved to be effective and environmentally friendly adsorbents for the removal of methylene blue, contributing to the development of sustainable solutions for water purification.

Keywords: Dye; Adsorption; Composite

RESUMO

O tratamento de efluentes e a descontaminação de corpos de água são desafios globais urgentes devido ao alto consumo de água e à geração de efluentes industriais. Este estudo desenvolveu adsorventes eficientes e econômicos para a remoção do azul de metileno, corante amplamente utilizado e de elevada

Published by Ciência e Natura under a CC BY-NC-SA 4.0 license.

toxicidade. Comp*ósitos* de quitosana e argila esmectita foram preparados e caracterizados utilizando análises de FTIR, XRD e pHpcz. O FTIR confirmou a preservação dos grupos funcionais de ambos os materiais no compósito preparado, enquanto os difratogramas indicaram uma interação superficial, evidenciada pela ausência de deslocamentos nos picos do difratograma. O pH do ponto de carga zero na superfície dos compósitos CS/Clay-180 e CS/Clay-580 foi avaliado como 8,5 e 8,4, respectivamente. Os experimentos de adsorção abrangeram uma faixa de pH de 3 a 11, tempos de exposição de até 600 minutos e concentração do corante de 5 a 350 mg L^{-1}. Os dados cinéticos seguiram modelos de primeira e segunda ordem, enquanto o modelo de Freundlich descreveu melhor as isotermas experimentais. Nossos comp*ósito*s apresentaram excelentes capacidades de adsorção, com valores máximos de 45,4 mg g^{-1} para CS/Clay-180 e 42,7 mg g^{-1} para CS/Clay-580, em pH 10 e tempo de contato de 300 min. Logo, as esferas de CS/Clay preparadas se apresentaram como adsorventes eficazes e ecologicamente corretos para a remoção de azul de metileno, contribuindo para o desenvolvimento de soluções sustentáveis para purificação de água.

Palavras-chave: Corante; Adsorção; Compósito

1 INTRODUCTION

Dyes, similar to other industrial effluents, are potential pollutants to bodies of water (Ewis et al., 2022; Goyal et al., 2023; Kwon & Kim, 2020; Methneni et al., 2021; Saba et al., 2021; Sirajudheen et al., 2021). They exhibit high toxicity, low degradability, and are carcinogenic (Singh et al., 2021). Additionally, they reduce sunlight penetration, thereby hindering photosynthesis and increasing Chemical Oxygen Demand (COD) (Rashid et al., 2020). These compounds are extensively used in various industries, including textiles, food, pharmaceuticals, paper and cosmetics (Basaleh et al., 2019; El-habacha et al., 2023).

Brazil ranks 5th in the world in textile production, with the Brazilian industry responsible for more than 1 million direct and 8 million indirect jobs (Vasconcelos et al., 2022). Despite the economic benefits, there are environmental concerns associated with the textile sector, as it is one of the largest consumers of water. Specifically, the dyeing and finishing stages are highlighted because they require up to 150 L of water to process 1 kg of cotton (Rashid et al., 2020). Another challenge is the minimal level of reuse, with a significant amount of waste being disposed of in the aquatic environment annually, often without appropriate treatment (Mittal et al., 2023).

While there are various methodologies for treating textile effluents, adsorption technology stands out for its practicality, efficiency, reuse of the adsorbent matrix, low investment capital, feasibility in removing toxic and degradation-resistant substances, and sludge-free cleanup operations (Badawi et al., 2021; Khan et al., 2020; Tran et al., 2023). In this context, new materials play a crucial role in the adsorption process of wastewater treatment, offering more efficient and specific solutions (de Oliveira et al., 2023; Duan et al., 2024; Theodoro da Rosa Salles et al., 2023). For example, Singhapong et al. (Singhapong et al., 2024) prepared a novel and reusable graphene oxide-coated reticulated open-cell mullite foams for methylene blue dye adsorption. The material developed and applied by the group exhibited excellent performance in removing this dye (the experimental results revealed that the materials can completely remove the dye from the aqueous solution within 30 min), making it a promising material for wastewater management. Another study highlighted the use of Fe_3O_4 nanoparticle/hyper-cross-linked polymer composites for dye removal (Gao et al., 2024). This work found that the prepared composite exhibited a high density of aromatic and alkyl groups, which conferred a high affinity for dyes through hydrophobic and π-π interactions. The results presented in this study reveal that this composite is a promising adsorbent for the removal of five dyes: Congo red, methyl orange, crystal violet, sunset yellow, and methylene blue.

The choice of the adsorbent matrix and the establishment of optimal operating conditions are critical in any adsorption process. Activated carbon is usually preferred due to its commercial availability, high surface area and adsorption capacity (Shen et al., 2018; Singh et al., 2021; Tran et al., 2023). However, it is not always the most cost-effective adsorbent and lacks selectivity. Alternatively, there are bioavailable materials with high saturation capacity, selectivity, and low cost that can be successfully used to remove various classes of contaminants (Biswas et al., 2021).

Figure 1 – Chitin deacetylation: Chitosan is obtained from chitin by immersing it in an alkaline solution at a temperature of 100°C, with constant stirring for approximately 4 hours, to achieve a lower degree of acetylation

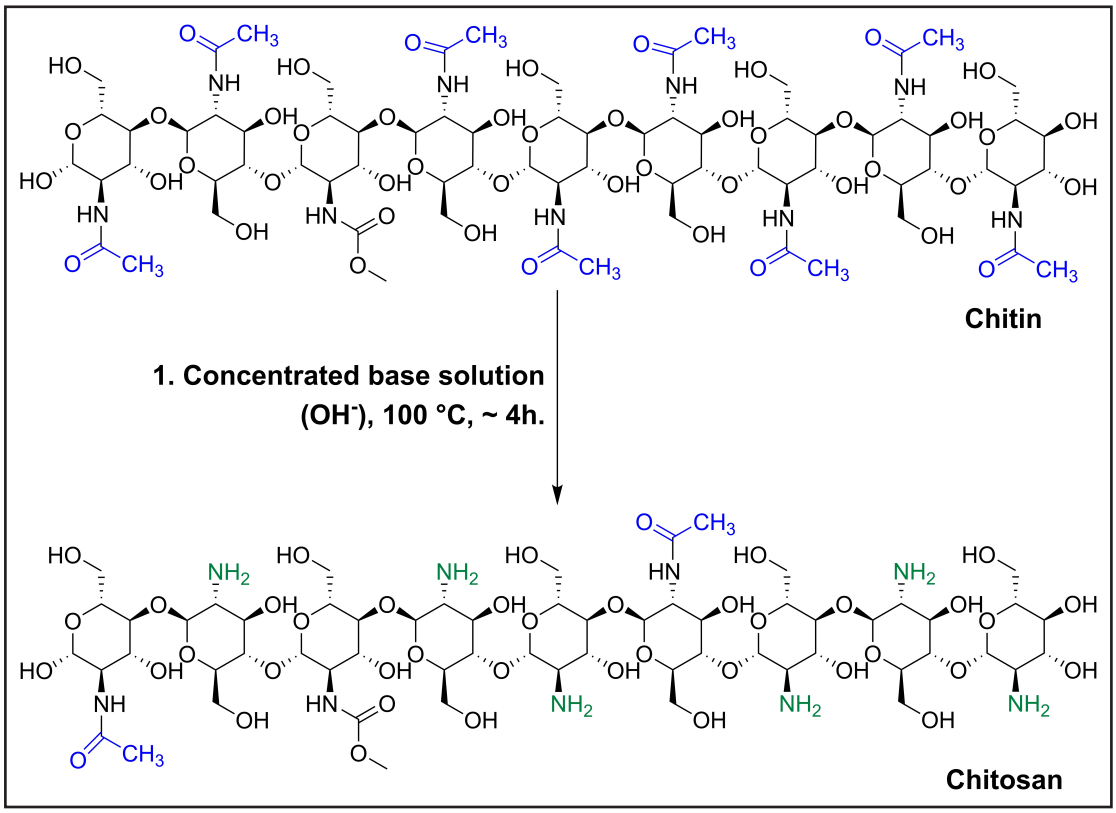

Source: Authors (2023)

One such example is a derivative of chitin, which is an abundant polysaccharide found in the exoskeleton of crustaceans (shrimps, crabs), insects and in the cell wall of yeasts. Through a simple process of deacetylation (Figure 1), chitin is transformed, to varying degrees, into chitosan (CS), a cationic polysaccharide (Marmier et al., 2020; Pakizeh et al., 2021). The degree of deacetylation and molar mass of the prepared CS depend on the concentration of the bases, temperature and reaction time.

Chitosan (CS) possesses favorable properties, being biodegradable, non-toxic, hydrophilic, chemically modifiable and selective in adsorption (Jawad & Abdulhameed, 2020; Nunes et al., 2021; Silva et al., 2021). However, its protonation and solubility at low pH levels (pH < 5.5, $pK_a \approx 6.5$) limit its direct use as an adsorbent (Zouaoui et al., 2020). Additionally, CS may exhibit low mechanical strength and a tendency to

form agglomerates (Jawad & Abdulhameed, 2020). Thus, there is a need to enhance its chemical properties, mechanical strength and adsorption capacity.

Various materials, including clays, can modify CS, expanding its insolubility range and adsorption capabilities. Clays are aluminosilicates with small particle size and high plasticity, offering versatile applications, including adsorption and strengthening of materials (Lertsutthiwong et al., 2012; Rekik et al., 2017; Rocha et al., 2014). Clays have good functionality and diverse applications, such as adsorbents, catalysts and for strengthening or improving the physical, mechanical, and structural properties of new materials (Jawad & Abdulhameed, 2020; Kausar et al., 2019; Marrakchi et al., 2020; Rekik et al., 2017). On the other hand, clay mining has a significant environmental consequence, prompting the exploration of methods to disperse clays in other matrices to reduce their environmental impact.

Among the various types of clay minerals, smectites are prominent. These clays possess a crystalline structure composed of octahedral silicate layers interleaved between tetrahedral layers, forming sheets separated by cation-containing intermediate layers (de Jong et al., 2014). Owing to their structural arrangement, smectites exhibit interesting properties such as swelling capacity and selective ion exchange (Christidis, 2008). This class of clay has been widely employed for contaminant adsorption owing to its inherent properties (Zhao et al., 2023). In addition, these clays have been utilized as precursor materials for the development of composites and hybrid materials (Mudzielwana & Gitari, 2021; Ouaddari et al., 2024).

CS-montmorillonite prepared through techniques like phase inversion and ion exchange, have been used in various fields, such as controlled release in agriculture for textile dye removal, selective electrode construction biodegradable packaging and bactericidal applications (Darder et al., 2003; Laaraibi et al., 2018; Lertsutthiwong et al., 2012; Messa et al., 2016). Other clays, such as kaolin, bentonite, attapulgite and sepiolite, have also been used to prepare hybrids with CS (Jawad & Abdulhameed, 2020; Kausar et al., 2019; Zhou et al., 2015).

This study extends the investigation into CS/Clay interactions, employing smectite clay standards (Clay-180 and Clay-580) and forming spherical hybrids. We evaluate the adsorption capacities of these materials against methylene blue (MB), a common cationic dye, while considering the influence of pH and time on the adsorption equilibria.

2 MATERIALS AND METHODS

2.1 Reagents and Solutions

All reagents used were of analytical grade. Methylene blue, potassium chloride (KCl), potassium bromide (KBr), and acetic acid (CH_3COOH) were all sourced from Isofar (Duque de Caxias, Brazil). Hydrochloric acid (HCl), and sodium hydroxide (NaOH) obtained from Quimex (Uberaba, Brazil), while Tonsil Supreme 180 FF (Clay-180) and Tonsil Terrana 580 FF (Clay-580) smectite clays were acquired from Clariant (Muttenz, Switzerland). Furthermore, CS with a degree of deacetylation ranging from 75% to 85% was purchased from Sigma-Aldrich (St.Louis, USA).

All the solutions were meticulously prepared using distilled water.

2.2 Preparation and Characterization of the Composites

To prepare the composites, 7 g of the Clay-180 smectite was added to 100 mL of a 2% m/V solution of CS and the mixture was stirred continuously for 24 h. Prior to this, the CS solution had been prepared in an acidic medium (5% V/V acetic acid) under constant stirring for 24 h. The resulting suspension, while still being stirred, was gradually added to an 8% m/V NaOH solution to induce precipitation and to form spheres, denoted as CS/Clay-180. These microspheres were subsequently filtered, washed until reaching a pH of 7 and dried in an oven at 50 °C for 24 h, following the procedure described in the literature (Messa et al., 2016; Vithalkar & Jugade, 2020). The same method was employed to obtain the CS/Clay-580 hybrid. Schematic representation of the preparation of the composites is presented in Figure 2.

Figure 2 – A schematic illustration of the preparation process for CS/Clay composites: (a) Solubilization of CS in CH_3COOH, (b) addition of clay to the previously prepared CS solution, (c) Precipitation of the CS/Clay dispersion into spheres in a NaOH solution, (d) filtration and washing of the formed spheres until the pH was close to 7, (e) drying of the materials in an oven for 24 h at 50 °C, and (f) illustration of the prepared composites in spherical form

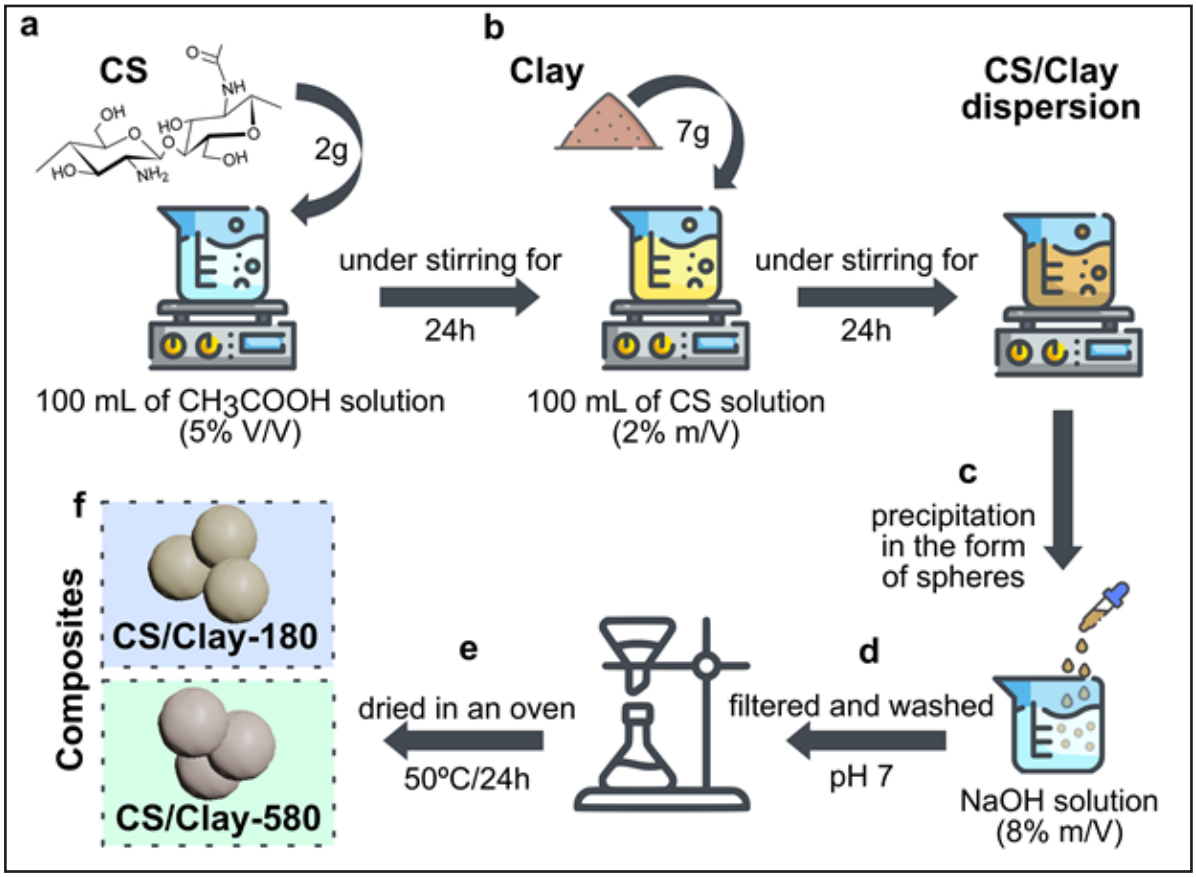

Source: Authors (2024)

Vibrational absorption spectra in the infrared region (4000 to 400 cm^{-1}) were acquired using an IR-PRESTIGE-20 spectrometer (Shimadzu, Kyoto, Japan). KBr chips (100 mg) were used and data was Fourier transformed with a resolution of 4 cm^{-1}.

XRD diffractograms were obtained using a D8-ADVANCE diffractometer (Bruker, Billerica, USA), operating at 40 kV and 30 mA. Copper served as the radiation source (Cu Kα, λ = 0.15405 nm), with a scanning range spanning from 3° to 75° and a scanning rate of 5° min^{-1}.

The pH at the point zero charge (pHpzc) was estimated using a graphical method based on pH equilibria in various solutions, while maintaining a constant ionic strength (Ribeiro et al., 2017). In summary, ten vials, each holding 100 mg of a designated adsorbent matrix, were exposed to 25 mL of pH solutions ranging from 3 to 12 (prepared using HCl and NaOH) in KCl (0.1 mol L^{-1}). pH measurements were conducted using a Q400AS pH meter (Quimis, Diadema, Brazil) with temperature correction. The systems were stirred at a constant temperature of 25 °C at 100 rpm, for 24 hours to ensure protonation equilibrium. After centrifugation, the pH values (pHf) of the supernatant were determined and the pHpzc was obtained from the plot of ΔpH (pHf – pHi) against pHi.

Methylene blue (MB) concentrations were determined using UV-Vis spectrophotometry. An IL-592S-BI spectrophotometer (Kasuaki, Tokyo, Japan) was used and concentrations were determined according to the respective analytical curves for each pH value, with a concentration range spanning from 10 to 100 mg L^{-1}.

Tukey's test was performed using the program PAST 4.0 (Øyvind Hammer et al., 2001) to evaluate the combinations of pH and CS/CLAY composites. Tukey's test is a statistical method that allows for pairwise comparisons of group means (Wade C. Driscoll, 1996), providing an honestly significant difference. For this purpose, 9 pH values (3-9) were combined with 2 composites (CS/CLAY-180 and CS/CLAY-580) and a control group (initial concentration), for a total of 19 groups. The PAST software was chosen for its robust statistical tools, which ensured the accuracy and reliability of our comparisons.

2.3 Adsorption Assays

Adsorption assays were conducted using a LUCA-222 shaker incubator (Lucadema, São José do Rio Preto, Brazil) with heating control. Each trial consisted of 50 mg of the adsorbent and 25 mL of the dye solution in the presence of an ionic

medium (0.1 mol L^{-1} KCl). The experiments were carried out at a controlled temperature of 25 °C, and with continuous stirring at 100 rpm. Detailed information regarding the parameters being investigated, their respective ranges and other experimental conditions can be found in Table 1.

The amount of adsorbed dye (q, mg g^{-1}) and the removal percentage (% R) were calculated using Equations 1 and 2, respectively (Kausar et al., 2019).

$$q = (C_i - C_f)\,V/m \quad (1)$$

$$\%R = (C_i - C_f)x\,100/C_i \quad (2)$$

Where C_i and C_f represent the initial and final dye concentrations (mg L^{-1}) respectively; V is the volume of dye solution (L) and m is the mass of the adsorbent (g)

Table 1 – Parameters, work ranges and experimental conditions for MB removal

Investigated parameters	Work ranges	Experimental conditions
Initial pH	3-11	Dye: 100 mg L^{-1} Time: 24 h
Time (min)	0-600	Dye: 100 mg L^{-1} pH = 10
Concentration (mg L^{-1})	5-350	pH = 10 Time: 300 min

Source: Authors (2023)

The kinetics experiments were conducted after determining the optimal adsorption pH. The results were fitted to first and second order kinetic models according to Equations 3 and 4 (Marrakchi et al., 2020):

$$q_t = q_{eq}(1 - e^{-k_1 t}) \quad (3)$$

$$q_t = \frac{k_2 q_{eq}^2 t}{1 + q_{eq} k_2 t} \quad (4)$$

Where q_t (mg g^{-1}) represents the adsorption capacity at time t (min); q_{eq} (mg g^{-1}) is the equilibrium adsorption capacity; k_1 (min^{-1}) and k_2 (mg g^{-1} min^{-1}) are the rate constants for the 1st and 2nd order kinetics, models, respectively.

The concentration study enabled the development of isotherms based on three well-established models: Langmuir (Eq. 5) (Langmuir, 1918), Freundlich (Eq. 6) (Kausar et al., 2019), and Sips (Eq. 7) (Sips, 1948).

Kinetic and isothermal modeling were conducted using nonlinear equations implemented in Microsoft Excel version 365 (Microsoft Corporation, Redmond WA, USA).

$$\frac{q_{eq}}{q_{max}} = \frac{K_L C_{eq}}{1 + K_L C_{eq}} \tag{5}$$

$$q_{eq} = K_f C_{eq}^{\frac{1}{n}} \tag{6}$$

$$q_{eq} = \frac{q_{max} K_s C_{eq}^{ns}}{1 + K_s C_{eq}^{ns}} \tag{7}$$

$$R_L = \frac{1}{1 + K_s C_0} \tag{8}$$

In these equations, q_{max} represents the maximum adsorbed amount (mg g^{-1}); C_0 (mg L^{-1}) denotes the initial concentration; C_{eq} (mg L^{-1}) signifies the concentration at equilibrium; K_L, K_F, K_s, and R_L are constants specific to the Langmuir, Freundlich, Sips models, with R_L being the dimensionless separation factor; n is the adsorption parameter in the Freundlich model, and n_s is the parameter associated with the adsorption site characteristics

3 RESULTS AND DISCUSSION

3.1 Vibrational Spectroscopy (FTIR)

The infrared vibrational spectra, shown in Figure 3, reveal distinct features. Notably, a broad band spanning from 3790 to 3000 cm^{-1} corresponds to NH and OH vibrations (Borja-Urzola et al., 2020). Vibrations at 3416 cm^{-1} are attributed to adsorbed water (Madejová, 2003), while the range from 2926 to 2841 cm^{-1} encompasses stretching

of the -CH group, deformation of methyl and methylene groups, and -NH stretching vibrations (Topcu et al., 2018).

An asymmetric stretching at 1643 cm^{-1} characterizes the C=O group of secondary amides, typical of the amide groups still present in CS (Madejová, 2003). AAdditionally, the vibrational stretch at 1420 cm-1 may be associated with the C-O bond within the carboxyl group (Cheikh et al., 2019). Angular deformation (δCH2) is evident at 1379 cm-1 (Cheikh et al., 2019), while asymmetrical vibrations at 1153 cm-1 indicate the presence of the C-O-C group in saccharides (Staroszczyk et al., 2014). Finally, amide III (νC-N, δNH) is observed at 1259 cm-1 (Santos et al., 2018).

Figure 3 – FTIR vibrational spectra of CS, Clay-180, Clay-580 and of the composites CS/Clay-180 and CS/Clay-580

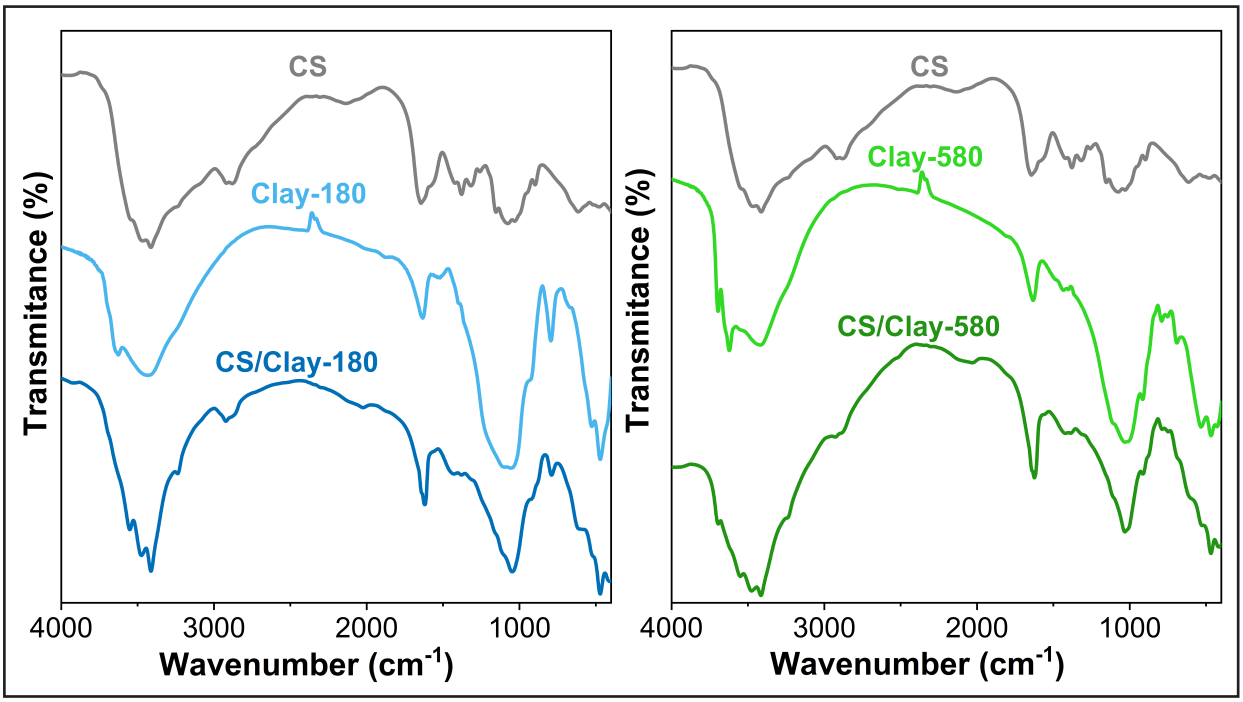

Source: Authors (2023)

Infrared spectroscopy revealed several significant bands in our clay samples. Bands at 3630 and 3435 cm-1 correspond to hydration water, while the 1633 cm-1 band is indicative of water molecules coordinated with exchangeable cations within

the clay matrix (Cheikh et al., 2019). Additionally, the 930 cm-1 band is associated with angular deformation in Al-Al-OH grouping, and the 795 cm-1 band pertains to Al-Mg-OH vibrations (Cacciotti et al., 2019; Cheikh et al., 2019). The spectral region spanning from 900 cm^{-1} to 1100 cm^{-1} signifies Si-O-Al bonds, forming the structural backbone of the clay (Iftikhar et al., 2020). Lastly, vibrations at 618, 515 and ≈ 450 cm^{-1} are attributed to coupled strains, encompassing Al-O, Si-O, Al-O-Si and Si-O-Si bands (Topcu et al., 2018). These preserved bands in the hybrids confirm the successful preparation route and the presence of characteristic clay functional groups, underscoring the other findings.

3.2 X-Ray Diffractometry (XRD)

Figure 4a and b depict the X-Ray diffractograms of the materials: CS, Clay-180, and Clay-580, as well as the composites: CS/Clay-180 and CS/Clay-580. Notably, CS exhibits two distinct reflection peaks at 2θ = 10° and 2θ = 20°, confirming the coexistence of hydrates and anhydrous crystals within its structure (Santos et al., 2018).

The Clay-180 diffraction pattern (Figure 4a) reveals distinct peaks at 2θ = 20.8º, 21.7º, 26.6º and 62.0° indicative of the presence of quartz (Jeon & Nam, 2019; Leite et al., 2000; Nizam El-Din & Ibraheim, 2021). Additionally, peaks at 2θ = 5.6º and 19.8°, characteristic of smectite (Leite et al., 2000; Rezende et al., 2012), are evident, alongside a peak at 2θ = 27.9°, attributed to calcium and potassium feldspar (Leite et al., 2000). Notably, these distinctive peaks are also observed in the diffraction pattern of the corresponding composite.

In contrast, the Clay-580 diffraction pattern (Figure 4b) displays peaks at 2θ = 8.8° and 29.6°, corresponding to montmorillonite (Jeon & Nam, 2019), at 2θ = 12.3°, characteristic of kaolinite (Rezende et al., 2012), at 2θ = 20.8°, indicating the presence of cristobalite (Rezende et al., 2012), and finally, at 2θ = 26.6°, a peak attributed to quartz present in the material (Jeon & Nam, 2019; Leite et al., 2000; Nizam El-Din & Ibraheim, 2021).

As previously observed, both Clay-180 and the corresponding composite exhibit their initial diffraction peaks at a similar angle of 5.68°. This pattern was also replicated in the case of Clay-580 and CS/Clay-580, with their diffraction peaks occurring at 2θ equal to 8.78°. TThis consistency allowed for the determination of the interplanar distance (d001) of these materials using the Bragg equation (Oliveira et al., 2011).

Figure 4 – Ray diffractograms: (a) CS, Clay-180, CS/Clay-180 composite and (b) CS, Clay-580, CS/Clay-580. (c) CS/Clays interaction model

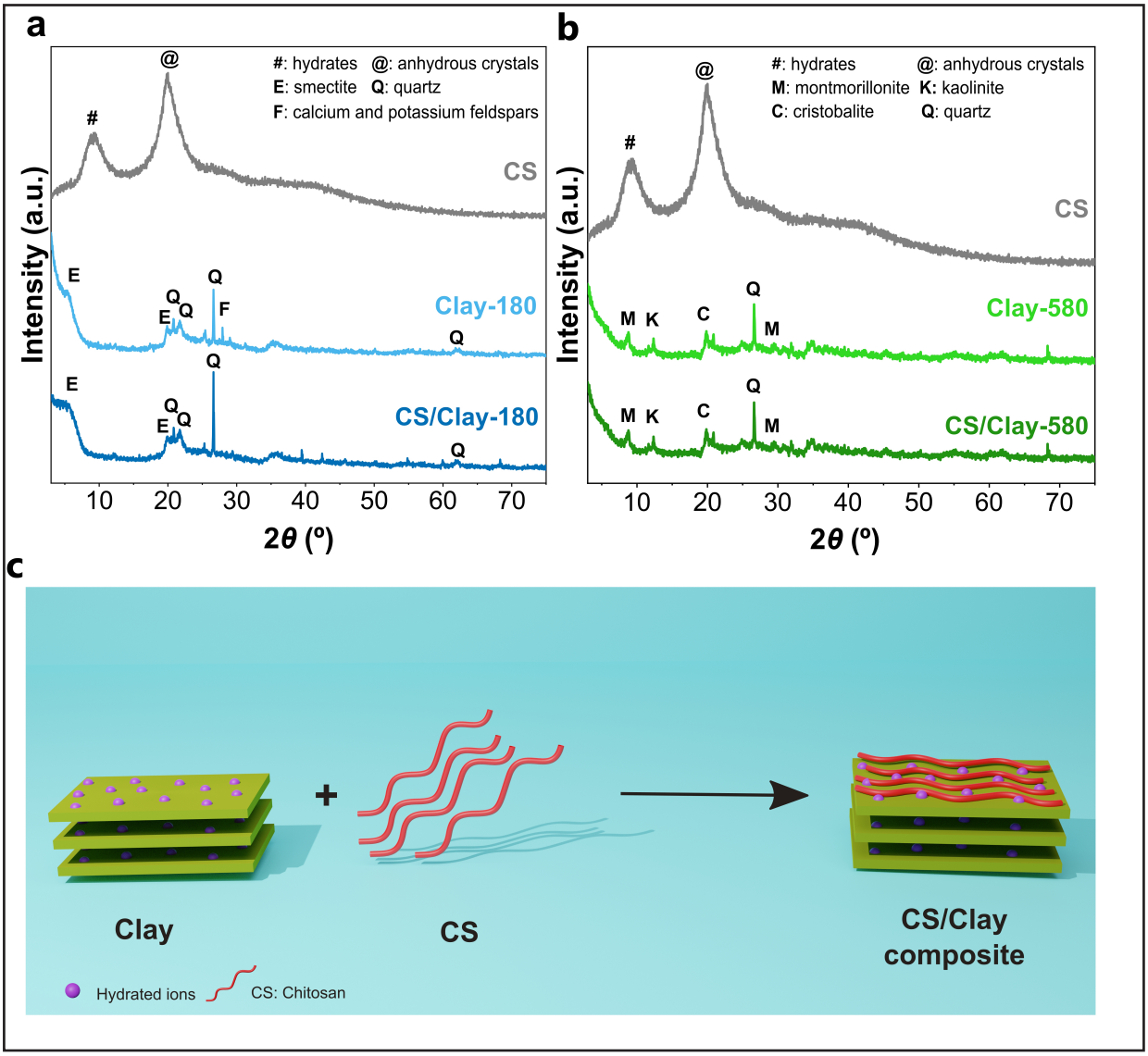

Source: Authors (2023)

The d001 value found for Clay-180 was identical to that of the composite CS/ Clay-180, measuring 1.55 nm. Likewise, both Clay-580 and the CS/Clay-580 composite

exhibited a d001 value of 1.01 nm. These findings indicate that, following the preparation of the composites, there were no new peaks formed, nor was there any noticeable shift in the d001 peak associated with the basal distance of the lamellae. This suggests that the interaction of CS with the clays was primarily confined to the surface, without causing any alteration to their lamellar structure. A simplified illustration of this process can be found in Figure 4c. The peaks that may have appeared to vanish after synthesis are likely a likely a result of the overlap between the clay peaks and the CS peaks in the formed hybrid, as previously discussed in the diffractograms presented in Figure 4a and b.

3.3 pH at zero charge point (pHpzc)

Determining the net charge on the adsorbent surface before the adsorption process is a crucial step that allows predicting in advance the pH conditions favoring interactions between the adsorbate and adsorbent. The concept of pHpzc refers to the pH at which the adsorbent attains a net electric charge density of zero. Below this pHpzc value, surface groups become protonated, leading to the migration of H^+ cations from the solution to the surface of the solid, thereby increasing the pH of the solution (pHi < pHf). Conversely, at pH values higher than pHpzc, the solvent removes H^+ ions from the surface, rendering it negatively charged and elevating the acidity (pHi > pHf) of the medium. The pHpzc for the materials studied are shown in Figure 5.

This approach facilitates the identification of optimal pH conditions for effective adsorption and provides a valuable framework for understanding the surface charge properties of the adsorbent materials.

The pHpzc values were determined to be from 1.3 to 3.1 for the Clay-180, 7.9 for Clay-580, 8.5 for CS/Clay-180, and 8.4 for CS/Clay-580 (Figure 5). It is noteworthy that the change in pHpzc for both clays became apparent after the formation of the hybrid materials, particularly for Clay-180, which exhibited an extended protonation range. These pHpzc values are consistent with those reported in the literature for similar composites. For instance, a composite with sodium bentonite exhibited a pHpzc of 7.8

(Anirudhan & Ramachandran, 2015)2015 and a composite involving a montmorillonite clay yielded a pHpzc of 7.3 (Bée et al., 2017).

Figure 5 – pH at zero charge point (pHpzc) for the starting materials (clays) and for the composites CS/Clay-180 and CS/Clay-580

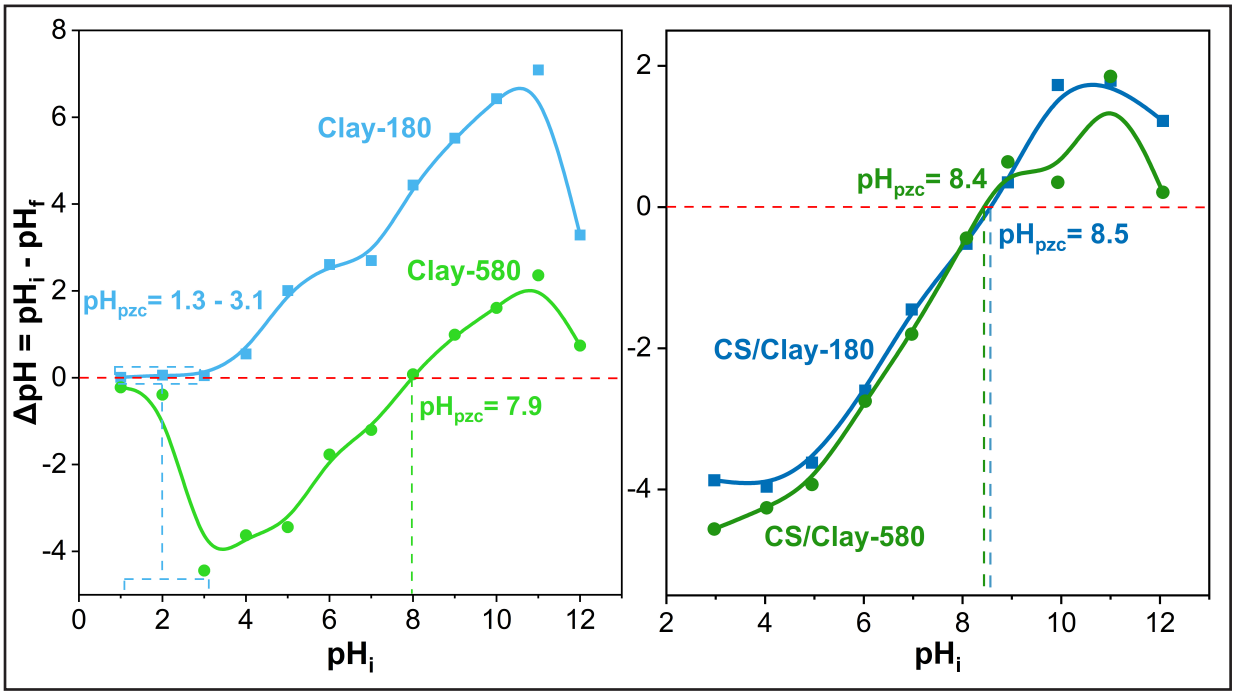

Source: Authors (2023)

These findings, in addition to confirming the modification of the material, suggest that these hybrid materials exhibit pHpzc values in a range similar to other known composites, underlining the relevance of these results in the context of adsorption processes and surface charge properties of the materials.

3.4 Adsorption assays: effect of initial pH

The investigation of the impact of pH on the removal of MB through adsorption by the composites was conducted within the pH range from 3 to 11, as depicted in Figure 6. Notably, the CS/Clay-180 composite demonstrated superior adsorptive performance, achieving its maximum removal capacity (39.27 mg g^{-1}). This finding is in line with results from a similar study involving CS composites with d-glucosamine and

n-acetyl-d-glucosamine/clay, which achieved maximum adsorption at pH 10 for the rose dye FRN (13.27 mg g^{-1}) (Kausar et al., 2019).

Conversely, the CS/Clay-580 composite displayed relatively consistent adsorption behavior across varying pH levels, with its maximum value at pH 11 (34.41 mg g^{-1}). Given that MB is a cationic dye, it was anticipated that stronger interactions with the solids would occur at pH values exceeding their respective pHpzc values. So, these results underscore the influence of pH on the adsorption capacity of the composites and highlight the potential utility of the CS/Clay-180 hybrid, particularly at a pH of 10, for effective removal of MB from solution.

Figure 6 – Amount of MB removed by the composites as a function of pH. Conditions: 50.0 mg of adsorbent; 25 mL of dye solution (100 mg L^{-1}, in KCl 0.1 mol L^{-1}); 25 ºC; stirring 100 rpm and contact time 24 h

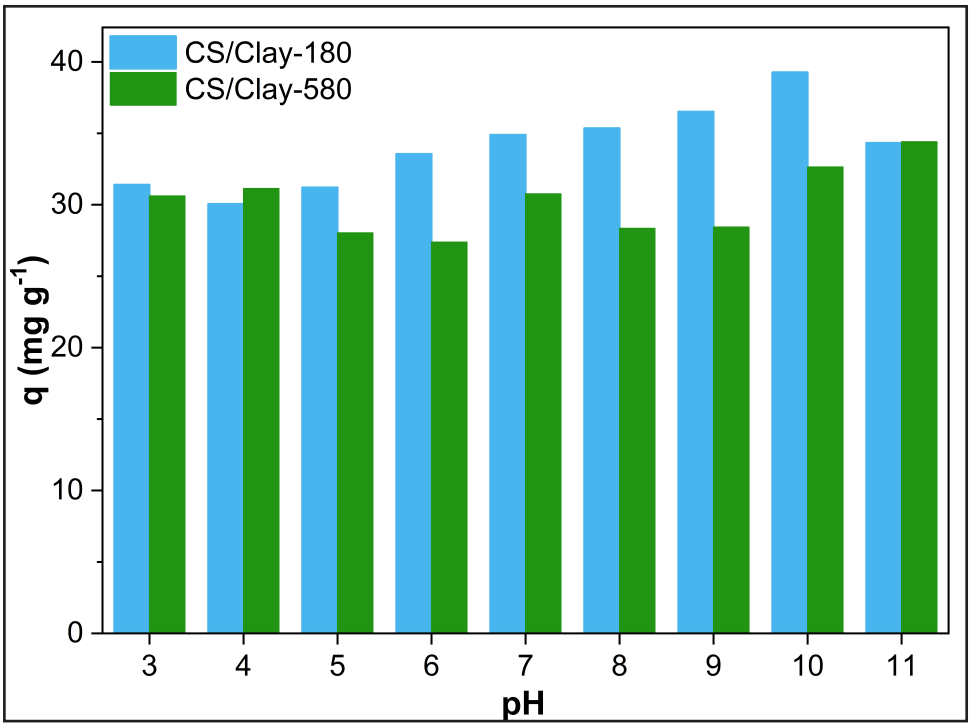

Source: Authors (2023)

Despite the heterogeneity and the presence of various functional groups identified through FTIR analysis (Figure 3), it is challenging to establish the exact mechanism of adsorption. However, we can infer possibilities based on the available

data. At a pH above 8.5, the adsorbent surfaces are deprotonated, as indicated by the pHpzc values. MB, being a cationic dye, undergoes deprotonation above its pK_a. Figure 7 provides a simplified adsorption scheme illustrating potential interaction between MB and the surfaces of the CS/Clay-180 and CS/Clay-580 at pH 10. In Figure 7, “a” represents hydrogen bonds, “b” denotes ion-dipole interactions, “c” signifies π-electron resonance, “d” implies dipole-dipole interactions, and “e” indicates electrostatic attraction.

Figure 7 – Possible interactions between composites and MB: a) hydrogen bonds; b) ion-dipole; c) electron resonance π; d) dipole-dipole; e) electrostatic attraction

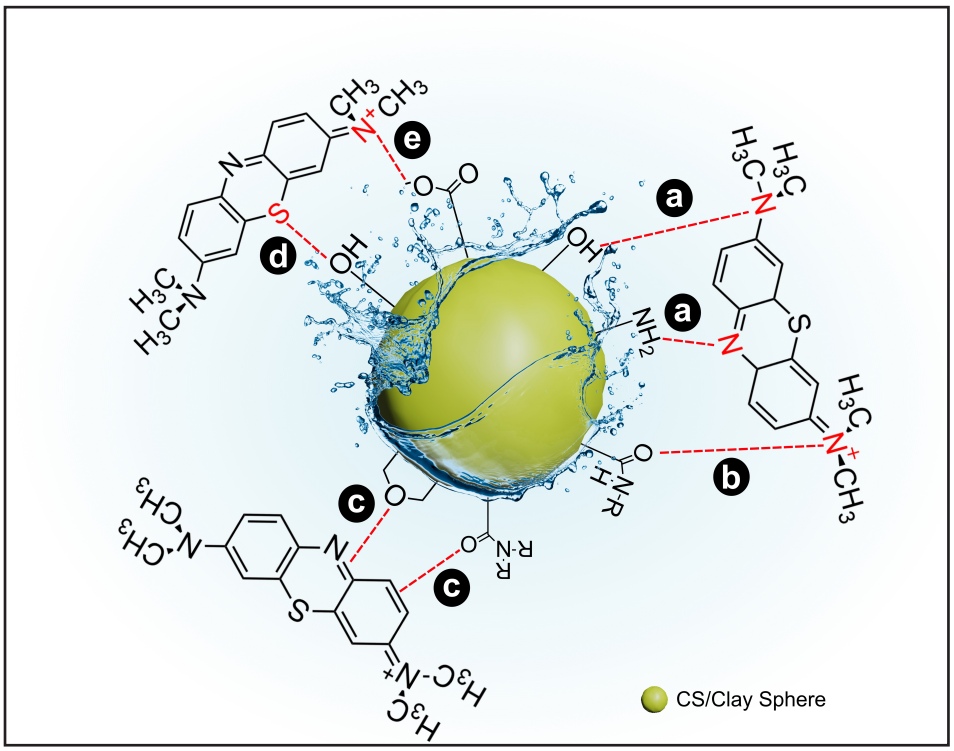

Source: Authors (2023)

3.5 Statistical Analysis

The radar chart (Figure 8) provides a visual representation of the treatment conditions, where each axis corresponds to independent variables such as pH and CS/CLAY combinations. The chart’s central region highlights the concentration of methylene blue, with the extreme right point showing the initial concentration of 100 mg L^{-1}. Other

points represent the dye concentrations after treatment under different pH values and CS/CLAY combinations. This visualization allows us to observe that, across similar pH conditions, the CS/CLAY-180 composite generally exhibited superior adsorption efficiency. The removal rates, which ranged from 60.2% to 78.6%, underscore the treatment's effectiveness, with notable similarities at certain pH levels (3, 4, 5, and 11).

Following this preliminary visual analysis, and aiming to determine the significance of variations in dye removal efficiency across different experimental conditions, one-way ANOVA (Analysis of Variance) with replication was performed. To Table 2 reveals a p-value < 0.05 and Fcal > Fcritical, indicating that dye removal significantly differed for at least one of the treatments. The combination of CS/CLAY and pH accounts for a substantial portion of the treatment effect and, additionally, the intraclass correlation coefficient (ICC) and effect size (ϖ^2) are close to one, supporting the treatment's statistical relevance (Table 2).

Figure 8 – Methylene blue concentrations at the beginning and after each experiment in the pH study

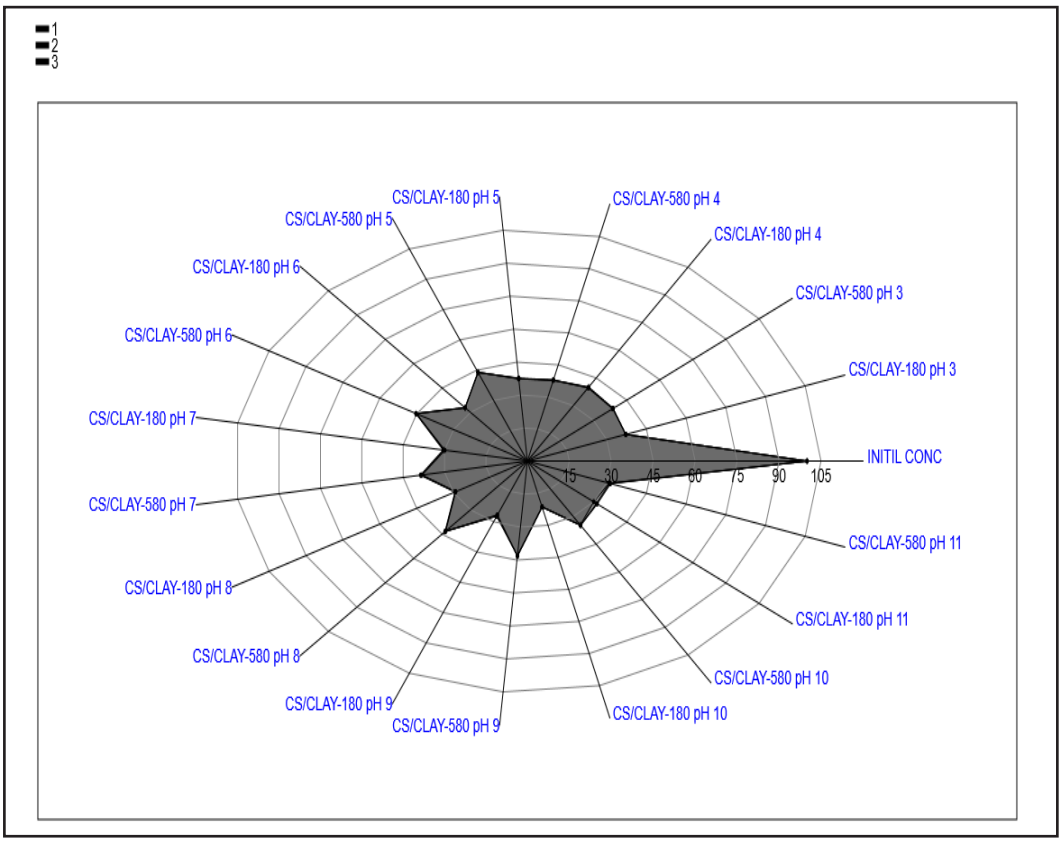

Source: Authors (2024)

Table 2 – ANOVA results for significant comparisons in the adsorption experiments (95% confidence interval)

Source of variation	SS [a]	DF [b]	MS [c]	F_{ratio}	$F_{critical}$	P_{value}	[d] ICC	[e] ϖ^2
Between groups	13898.7	18	772.15	1.21×10^4	1.96 - 1.84	1.04×10^{-65}	0.99975	0.9997
Within groups	2.44824	38	0.0644					
Total	13901.1	56	1.00×10^{-05}					

[a] Sum square, [b] degrees of freedom, [c] mean square, [d] intraclass correlation coefficient, [e] effect size. Source: Authors (2024)

Post-hoc analysis with Tukey's HSD test was applied to perform pairwise comparisons between treatment combinations. The objective was to identify which specific pairs exhibited statistically significant differences in adsorption rates. The analysis revealed that a large majority of the treatment combinations showed statistically significant differences, with p-values less than 0.05. This indicates that variations in pH levels and CS/CLAY combinations significantly influenced adsorption efficiency. Out of the total comparisons (n=171), 163 combinations demonstrated significant differences in their mean adsorption rates.

However, there were a few combinations (n=8) where no significant statistical differences were observed, as detailed in Table 3. These combinations had p-values greater than 0.05, indicating similar adsorption efficiencies and suggesting similar adsorption behavior under certain conditions, which may point to optimal ranges or saturation points for these variables or consistent behavior across certain pH levels and CS/CLAY types. High p-values ($p \approx 1$) indicate that there is a high chance that the observed difference between the means is not significant.

Table 3 – Tukey's test results for adsorption efficiency: non-statistically significant comparisons (p-value > 0.05)

Comparison CS/CLAY types	Mean difference	p-value
CS/CLAY-180; pH 3 (37.2) and CS/CLAY-580; pH 4 (37.7)	0.5	0.219
CS/CLAY-180; pH 3 (37.2) and CS/CLAY-180 pH 5 (37.6)	0.4	0.945
CS/CLAY-580; pH 3 (38.8) and CS/CLAY-580; pH 7 (38.5)	0.3	0.994
CS/CLAY-580; pH 4 (37.7) and CS/CLAY-180; pH 5 (37.6)	0.1	0.997
CS/CLAY-580; pH 4 (37.7) and CS/CLAY-580; pH 7 (38.5)	0.8	0.239
CS/CLAY-580; pH 5 (43.9) and CS/CLAY-580; pH 8 (43.3)	0.6	0.247
CS/CLAY-580; pH 8 (43.3) and CS/CLAY-580; pH 9 (43.1)	0.2	1
CS/CLAY-180; pH 11 (31.3) and CS/CLAY-580; pH 11 (31.2)	0.1	1

Mean concentrations (mg L^{-1}) after treatment are shown in parenthese

3.6 Adsorption Kinetics

The choice of pH 10 (Figure 6) as the optimum pH for adsorption aimed to maximize dye removal. Kinetic studies play a crucial role in understanding contact time, removal rates, and the efficiency of the adsorption process. The experimental results and plots for the non-linearized pseudo-first and pseudo-second-order models are presented in Figure 9. It is evident that equilibrium was reached at approximately 300 minutes.

The linearized kinetic modeling results (as shown in Table 4) indicated that the pseudo-first order model provides the best description of the experimental data for the CS/Clay-180 composite. This observation is coherent with the notion that the removal rate primarily depends on the number of active sites available on the adsorbent.

Figure 9 – Contact time and adsorption kinetics of MB (100 mg L^{-1}) by CS/Clay-180 and CS/Clay-580 composites at pH 10

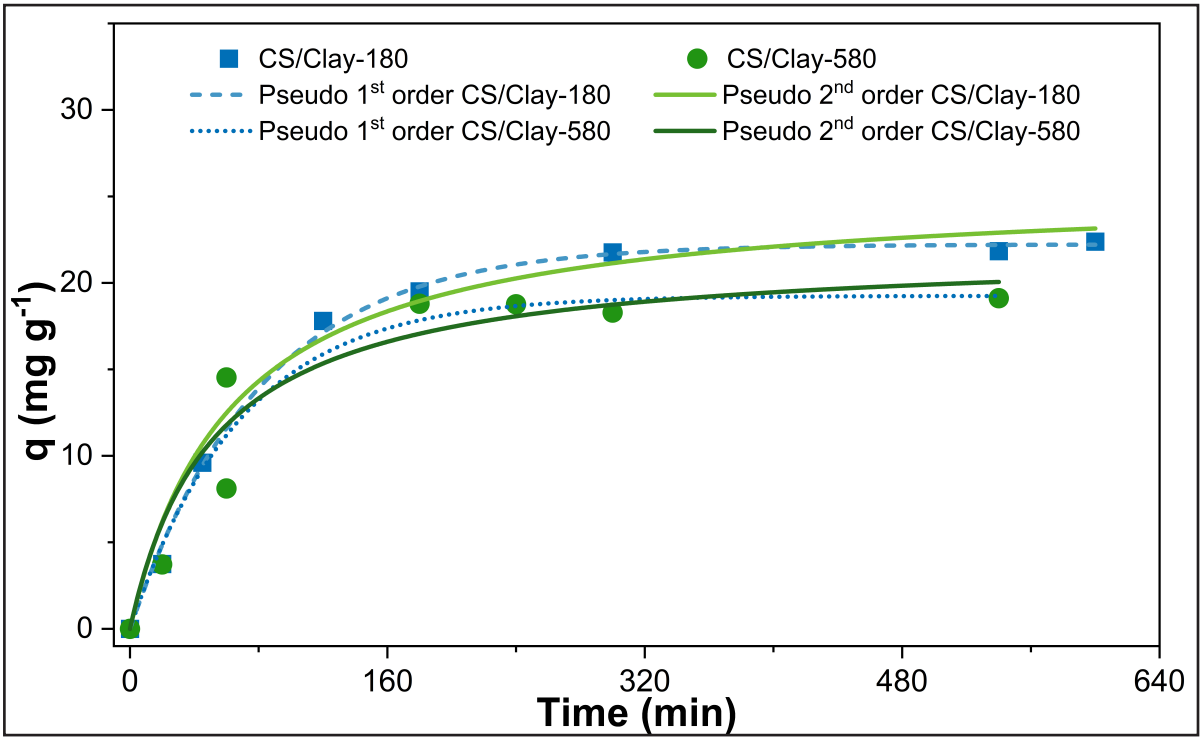

Source: Authors (2023)

Table 4 – Results of the fits for the first and second order linearized models on MB removal for CS/Clay-180 and CS/Clay-580

Composite	*$Re_{exp.}$	1st order			2nd order		
	mg g^{-1}	k_1 min^{-1}	**$Re_{teo.}$ mg g^{-1}	R^2 -	k_2 mg g^{-1} min^{-1}	$Re_{teo.}$ mg g^{-1}	R^2 -
CS/Clay-180	22.1	$1.23x10^{-2}$	22.2	0.996	$6.22x10^{-4}$	25.6	0.982
CS/Clay-580	18.7	$1.45x10^{-2}$	19.3	0.934	$8.76x10^{-4}$	22.0	0.980

* Experimental removal rate, **theoretical removal rate. Source: Authors (2023)

In contrast, for the CS/Clay-580 composite, the linearized kinetic modeling indicated that the pseudo-second order model provided the best fit to the experimental data, with the R^2 value exceeding 0.98, confirming a very strong correlation. The experimental values align well with the calculated values (as shown in Table 4), and

the low values of k_1 and k_2 further support the idea that it takes a significant time to saturate the adsorbent surface (300 min).

3.7 Adsorption Isotherm

Following the determination of the optimum pH (pH 10) and equilibrium time (300 min), adsorption isotherms were obtained to further understand the adsorption behavior. presents the experimental data along with non-linear plots for the Langmuir, Freundlich, and Sips models (Figure 10).

The presence of a plateau, indicating saturation of the adsorbent, made it challenging to definitively select the best adsorption model. However, all models exhibited R^2 values exceeding 95%. Although the Langmuir model displayed a relatively good fit with approximately 96%, there were substantial deviations between the experimental and theoretical adsorbed amounts (q), amounting to 43.6% for CS/Clay-180 and 56.4% for CS/Clay-580.

Figure 10 – Adsorption isotherms of MB by CS/Clay-180 and CS/Clay-580 composites at pH 10

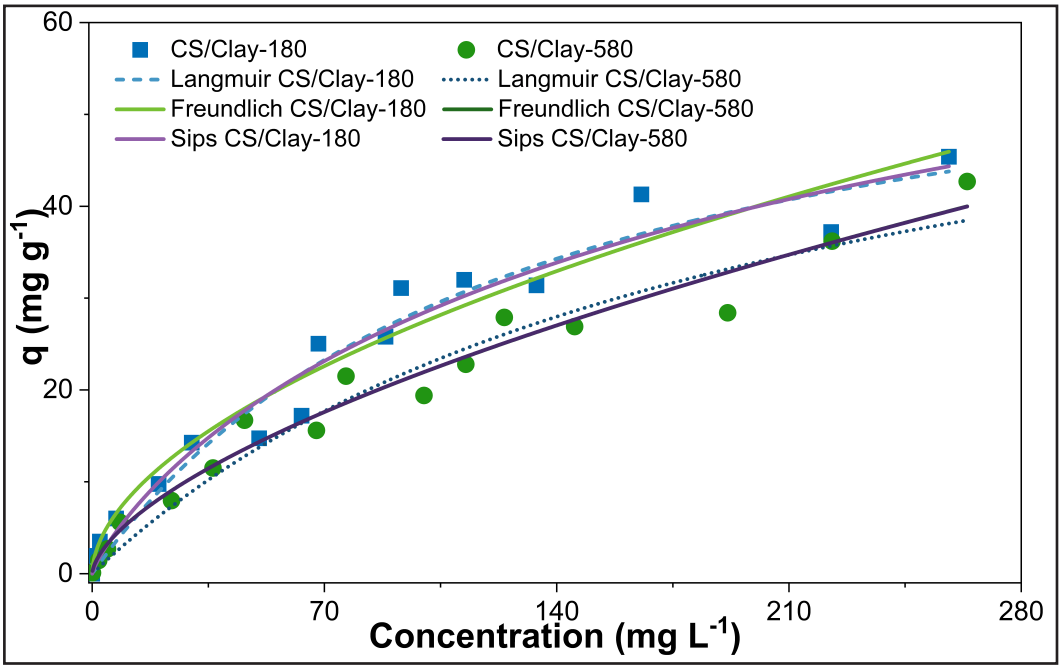

Source: Authors (2023)

Similar observations apply to the Sips model, which combines parameters from both the Freundlich and Langmuir models and yields larger deviations. The absence of the plateau (monolayer) and slight curvature observed in the isotherms suggests favorable adsorption behavior, where the removal of the analyte per unit mass of adsorbent remains high even at low analyte concentrations at equilibrium. It is essential to note that the Langmuir model assumes energetically identical sites (Alafnan et al., 2021; Hu et al., 2023), a concept that may not apply to this study given the heterogeneity of the matrix, as shown in Figure 3 and Figure 7. Additionally, when the separation factor (R_L) is 1, the isotherm tends to be linear. In summary, while the adsorption isotherms presented challenges in fitting the Langmuir and Sips models precisely, the deviations observed may be attributed to the heterogeneous nature of the matrix and the unique characteristics of the adsorbents and adsorbate interactions in this study.

Table 5 – Results of isotherm mode adjustments

Model	CS/Clay-180					CS/Clay-580				
	*$q_{exp.}$	$q_{teo.}$	K_L, F, S	R_L / n	R^2	$q_{exp.}$	$q_{teo.}$	K_L, F, S	R_L / n	R^2
Langmuir	45.4	65.2	$7.93x10^{-3}$	0.962 / -	0.961	42.7	66.8	$5.15x10^{-3}$	0.975 / -	0.957
Freundlich	45.4	-	2.25	- / 1.84	0.956	42.7	-	1.27	- / 1.62	0.971
Sips	45.4	82.9	$1.12x10^{-2}$	- / 0.834	0.959	42.7	5709	$2.21x10^{-4}$	- / 0.621	0.968

*Units of the displayed parameters: q (mg g^{-1}), K_L (L mg^{-1}), KF ($mg^{1-1/n}$ $L^{1/n}$ g^{-1}), K_S (L mg^{-1}). Source: Authors (2023)

The Freundlich model is particularly suitable for describing adsorption on heterogeneous solids with multiple active sites, each having distinct energy levels (Chen et al., 2022). This model accounts for multilayer adsorption and does not impose a strict limit on the maximum adsorption capacity (q_{eq}) concerning the equilibrium concentration (C_{eq}). However, it is important to recognize that, in practice, there are

limits to how much q_{eq} can increase with increasing C_{eq}, and excessively high values of q_{eq} and C_{eq} can lead to distortions in the model. Low values of the Freundlich parameter "n" (as shown in Table 5) suggest the presence of sites with lower energy and, consequently, weaker adsorbent/adsorbate interactions. Furthermore, it suggests that the Freundlich model is the most suitable for describing the isotherm in this context for CS/Clay-180 (R^2 = 0.956) CS/Clay-580 (R^2 = 0.971). The results presented in Table 5, along with the arguments provided, indicate that the hybrid CS/Clay-180 exhibited a higher adsorption rate of MB.

4 CONCLUSIONS

This study successfully prepared composites using straightforward and mild conditions, resulting in materials well-characterized by FTIR, XRD, and pHpzc analyses. These materials were evaluated for their adsorption properties, specifically targeting cationic methylene blue dye, while considering the effects of pH, contact time, and dye concentration. The characterization revealed interactions between the clays and chitosan, which remained intact regardless of pH conditions and being in an aqueous medium. The adsorption process displayed pH dependency, with optimal adsorption observed at pH 10 (Clay-180) and 11 (Clay-580). Kinetic studies indicated an equilibrium time of approximately 300 minutes and the first-order kinetic mechanism provided the best correlation with the experimental results. In the realm of adsorption equilibrium studies, the Langmuir, Freundlich, and Sips models yielded comparable correlations. The Freundlich model, fitted the data best, suggests multilayer adsorption on heterogeneous surfaces, for the CS/Clay-180 and CS/Clay-580 hybrids. In view of the good performance of the composites in removing MB dye, future studies related to the desorption and reuse processes of the composites are necessary to provide a more comprehensive view of the long-term efficiency of the adsorbents studied in

this work. These findings contribute to our understanding of the adsorption behavior of these composites, highlighting their potential utility in various environmental and wastewater treatment applications.

ACKNOWLEDGEMENTS

The authors would like to thank the Maranhão Research Foundation (*Fundação de Amparo à Pesquisa e ao Desenvolvimento Científico e Tecnológico do Maranhão* - FAPEMA) for their financial support.

REFERENCES

Alafnan, S., Awotunde, A., Glatz, G., Adjei, S., Alrumaih, I., & Gowida, A. (2021). Langmuir adsorption isotherm in unconventional resources: Applicability and limitations. *Journal of Petroleum Science and Engineering*, *207*, 109172. Recovered from: https://doi.org/10.1016/j.petrol.2021.109172

Anirudhan, T. S., & Ramachandran, M. (2015). Adsorptive removal of basic dyes from aqueous solutions by surfactant modified bentonite clay (organoclay): Kinetic and competitive adsorption isotherm. *Process Safety and Environmental Protection*, *95*, 215–225. Recovered from: https://doi.org/10.1016/j.psep.2015.03.003

Badawi, A. K., Elkodous, M. A., & Ali, G. A. M. (2021). Recent advances in dye and metal ion removal using efficient adsorbents and novel nano-based materials: An overview. *RSC Advances*, *11*(58), 36528–36553. Recovered from: https://doi.org/10.1039/D1RA06892J

Basaleh, A. A., Al-Malack, M. H., & Saleh, T. A. (2019). Methylene Blue removal using polyamide-vermiculite nanocomposites: Kinetics, equilibrium and thermodynamic study. *Journal of Environmental Chemical Engineering*, *7*(3), 103107. Recovered from: https://doi.org/10.1016/j.jece.2019.103107

Bée, A., Obeid, L., Mbolantenaina, R., Welschbillig, M., & Talbot, D. (2017). Magnetic chitosan/clay beads: A magsorbent for the removal of cationic dye from water. *Journal of Magnetism and Magnetic Materials*, *421*, 59–64. Recovered from: https://doi.org/10.1016/j.jmmm.2016.07.022

Biswas, S., Fatema, J., Debnath, T., & Rashid, T. U. (2021). Chitosan–Clay Composites for Wastewater Treatment: A State-of-the-Art Review. *ACS ES&T Water*, *1*(5), 1055–1085. Recovered from: https://doi.org/10.1021/acsestwater.0c00207

Borja-Urzola, A. del C., García-Gómez, R. S., Flores, R., & Durán-Domínguez-de-Bazúa, M. del C. (2020). Chitosan from shrimp residues with a saturated solution of calcium chloride in methanol and water. *Carbohydrate Research*, *497*, 108116. Recovered from: https://doi.org/10.1016/j.carres.2020.108116

Cacciotti, I., Lombardelli, C., Benucci, I., & Esti, M. (2019). Clay/chitosan biocomposite systems as novel green carriers for covalent immobilization of food enzymes. *Journal of Materials Research and Technology*, *8*(4), 3644–3652. Recovered from: https://doi.org/10.1016/j.jmrt.2019.06.002

Cheikh, D., García-Villén, F., Majdoub, H., Zayani, M. B., & Viseras, C. (2019). Complex of chitosan pectin and clay as diclofenac carrier. *Applied Clay Science*, *172*, 155–164. Recovered from: https://doi.org/10.1016/j.clay.2019.03.004

Chen, X., Hossain, M. F., Duan, C., Lu, J., Tsang, Y. F., Islam, M. S., & Zhou, Y. (2022). Isotherm models for adsorption of heavy metals from water - A review. *Chemosphere*, *307*, 135545. Recovered from: https://doi.org/10.1016/j.chemosphere.2022.135545

Christidis, G. E. (2008). Validity of the structural formula method for layer charge determination of smectites: A re-evaluation of published data. *Applied Clay Science*, *42*(1), 1–7. Recovered from: https://doi.org/10.1016/j.clay.2008.02.002

Darder, M., Colilla, M., & Ruiz-Hitzky, E. (2003). Biopolymer−Clay Nanocomposites Based on Chitosan Intercalated in Montmorillonite. *Chemistry of Materials*, *15*(20), 3774–3780. Recovered from: https://doi.org/10.1021/cm0343047

Duan, F., Zhu, Y., Liu, Y., Mu, B., & Wang, A. (2024). Green Fabrication of Porous Adsorbent with Structural Evolution of Mixed-Dimension Attapulgite Clay for Efficient Removal of Methylene Blue and Sustainable Utilization. *ACS Sustainable Resource Management*, *1*(4), 670–680. Recovered from: https://doi.org/10.1021/acssusresmgt.3c00086

El-habacha, M., Miyah, Y., Lagdali, S., Mahmoudy, G., Dabagh, A., Chiban, M., Sinan, F., ... & Zerbet, M. (2023). General overview to understand the adsorption mechanism of textile dyes and heavy metals on the surface of different clay materials. *Arabian Journal of Chemistry*, *16*(11), 105248. Recovered from: https://doi.org/10.1016/j.arabjc.2023.105248

Ewis, D., Ba-Abbad, M. M., Benamor, A., & El-Naas, M. H. (2022). Adsorption of organic water pollutants by clays and clay minerals composites: A comprehensive review. *Applied Clay Science*, *229*, 106686. Recovered from: https://doi.org/10.1016/j.clay.2022.106686

Gao, L., Lu, Y., Chen, S., Ma, X., & Zhao, W. (2024). Fe3O4 Nanoparticle/Hyper-Cross-Linked Polymer Composites for Dye Removal. *ACS Applied Nano Materials*, *7*(9), 9960–9967. Recovered from: https://doi.org/10.1021/acsanm.3c06264

Goyal, N., Amar, A., Gulati, S., & Varma, R. S. (2023). Cyclodextrin-Based Nanosponges as an Environmentally Sustainable Solution for Water Treatment: A Review. *ACS Applied Nano Materials*, *6*(15), 13766–13791. Recovered from: https://doi.org/10.1021/acsanm.3c02026

Hammer, Ø., Harper, D. & Ryan, P. D. (2001). PAST: PALEONTOLOGICAL STATISTICS SOFTWARE PACKAGE FOR EDUCATION AND DATA ANALYSIS. *Paleontologia Eletrônica*, *4*(1). Recovered from: https://palaeo-electronica.org/2001_1/past/issue1_01.htm

Hu, Q., Lan, R., He, L., Liu, H., & Pei, X. (2023). A critical review of adsorption isotherm models for aqueous contaminants: Curve characteristics, site energy distribution and common controversies. *Journal of Environmental Management*, *329*, 117104. Recovered from: https://doi.org/10.1016/j.jenvman.2022.117104

Iftikhar, S., Rashid, K., Ul Haq, E., Zafar, I., Alqahtani, F. K., & Iqbal Khan, M. (2020). Synthesis and characterization of sustainable geopolymer green clay bricks: An alternative to burnt clay brick. *Construction and Building Materials*, *259*, 119659. Recovered from: https://doi.org/10.1016/j.conbuildmat.2020.119659

Jawad, A. H., & Abdulhameed, A. S. (2020). Facile synthesis of crosslinked chitosan-tripolyphosphate/kaolin clay composite for decolourization and COD reduction of remazol brilliant blue R dye: Optimization by using response surface methodology. *Colloids and Surfaces A: Physicochemical and Engineering Aspects*, *605*, 125329. Recovered from: https://doi.org/10.1016/j.colsurfa.2020.125329

Jong, S. M. de, Spiers, C. J., & Busch, A. (2014). Development of swelling strain in smectite clays through exposure to carbon dioxide. *International Journal of Greenhouse Gas Control*, *24*, 149–161. Recovered from: https://doi.org/10.1016/j.ijggc.2014.03.010

Jeon, I., & Nam, K. (2019). Change in the site density and surface acidity of clay minerals by acid or alkali spills and its effect on pH buffering capacity. *Scientific Reports*, *9*(1), Article 1. Recovered from: https://doi.org/10.1038/s41598-019-46175-y

Kausar, A., Naeem, K., Hussain, T., Nazli, Z.-H., Bhatti, H. N., Jubeen, F., Nazir, A., & Iqbal, M. (2019). Preparation and characterization of chitosan/clay composite for direct Rose FRN dye removal from aqueous media: Comparison of linear and non-linear regression methods. *Journal of Materials Research and Technology*, *8*(1), 1161–1174. Recovered from: https://doi.org/10.1016/j.jmrt.2018.07.020

Khan, M. S., Khalid, M., & Shahid, M. (2020). What triggers dye adsorption by metal organic frameworks? The current perspectives. *Materials Advances*, *1*(6), 1575–1601. Recovered from: https://doi.org/10.1039/D0MA00291G

Kwon, D., & Kim, J. (2020). Silver-doped ZnO for photocatalytic degradation of methylene blue. *Korean Journal of Chemical Engineering*, *37*(7), 1226–1232. Recovered from: https://doi.org/10.1007/s11814-020-0520-7

Laaraibi, A., Moughaoui, F., Damiri, F., Ouakit, A., Charhouf, I., Hamdouch, S., Jaafari, A., ... & Berrada, A. B. (2018). Chitosan-Clay Based (CS-NaBNT) Biodegradable Nanocomposite Films for Potential Utility in Food and Environment. In Dongre, Rejendra. *Chitin-Chitosan—Myriad Functionalities in Science and Technology*. IntechOpen. Recovered https://doi.org/10.5772/intechopen.76498

Langmuir, I. (1918). The Adsorption of Gases on Plane Surfaces of Glass, Mica and Platinum. *Journal of the American Chemical Society*, *40*(9), 1361–1403. Recovered from: https://doi.org/10.1021/ja02242a004

Leite, S. Q. M., Colodete, C. H. A., Dieguez, L. C., & San Gil, R. A. S. (2000). Extração de ferro de esmectita brasileira com emprego do método ditionito-citrato-bicarbonato. *Química Nova*, *23*, 297–302. Recovered from: https://doi.org/10.1590/S0100-40422000000300002

Lertsutthiwong, P., Noomun, K., Khunthon, S., & Limpanart, S. (2012). Influence of chitosan characteristics on the properties of biopolymeric chitosan–montmorillonite. *Progress in Natural Science: Materials International*, *22*(5), 502–508. Recovered from: https://doi.org/10.1016/j.pnsc.2012.07.008

Madejová, J. (2003). FTIR techniques in clay mineral studies. *Vibrational Spectroscopy*, *31*(1), 1–10. Recovered from: https://doi.org/10.1016/S0924-2031(02)00065-6

Marmier, T., Szczepanski, C. R., Candet, C., Zenerino, A., Godeau, R.-P., & Godeau, G. (2020). Investigation on Mecynorhina torquata Drury, 1782 (Coleoptera, Cetoniidae, Goliathini) cuticle: Surface properties, chitin and chitosan extraction. *International Journal of Biological Macromolecules*, *164*, 1164–1173. Recovered from: https://doi.org/10.1016/j.ijbiomac.2020.07.155

Marrakchi, F., Hameed, B. H., & Hummadi, E. H. (2020). Mesoporous biohybrid epichlorohydrin crosslinked chitosan/carbon–clay adsorbent for effective cationic and anionic dyes adsorption. *International Journal of Biological Macromolecules*, *163*, 1079–1086. Recovered from: https://doi.org/10.1016/j.ijbiomac.2020.07.032

Messa, L. L., Froes, J. D., Souza, C. F., & Faez, R. (2016). Híbridos de Quitosana-Argila para Encapsulamento e Liberação Sustentada do Fertilizante Nitrato de Potássio. *Química Nova*, *39*, 1215–1220. Recovered from: https://doi.org/10.21577/0100-4042.20160133

Methneni, N., Morales-González, J. A., Jaziri, A., Mansour, H. B., & Fernandez-Serrano, M. (2021). Persistent organic and inorganic pollutants in the effluents from the textile dyeing industries: Ecotoxicology appraisal via a battery of biotests. *Environmental Research*, *196*, 110956. Recovered from: https://doi.org/10.1016/j.envres.2021.110956

Mittal, H., Alili, A. A., & Alhassan, S. M. (2023). Latest progress in utilizing gum hydrogels and their composites as high-efficiency adsorbents for removing pollutants from wastewater. *Journal of Molecular Liquids*, *391*, 123392. Recovered from: https://doi.org/10.1016/j.molliq.2023.123392

Mudzielwana, R., & Gitari, M. W. (2021). Removal of fluoride from groundwater using MnO2 bentonite-smectite rich clay soils composite. *Groundwater for Sustainable Development*, *14*, 100623. Recovered from: https://doi.org/10.1016/j.gsd.2021.100623

Nizam El-Din, H. M., & Ibraheim, D. M. (2021). Biological applications of nanocomposite hydrogels prepared by gamma-radiation copolymerization of acrylic acid (AAc) onto plasticized starch (PLST)/montmorillonite clay (MMT)/chitosan (CS) blends. *International Journal of Biological Macromolecules*, *192*, 151–160. Recovered from: https://doi.org/10.1016/j.ijbiomac.2021.09.196

Nunes, Y. L., Menezes, F. L. de, Sousa de, I. G., Cavalcante, A. L. G., Cavalcante, F. T. T., Silva Moreira, K. da, Oliveira, A. L. B. de, ... & Santos, J. C. S. dos. (2021). Chemical and physical Chitosan modification for designing enzymatic industrial biocatalysts: How to choose the best strategy? *International Journal of Biological Macromolecules*, *181*, 1124–1170. Recovered from: https://doi.org/10.1016/j.ijbiomac.2021.04.004

Oliveira, M. F. L. de, Oliveira, M. G. de, & Leite, M. C. A. M. (2011). Nanocompósitos de poliamida 6 e argila organofílica: Estudo da cristalinidade e propriedades mecânicas. *Polímeros*, *21*, 78–82. Recovered from: https://doi.org/10.1590/S0104-14282011005000015

Oliveira, M. P. de, Schnorr, C., Rosa Salles, T. da, Silva Bruckmann, F. da, Baumann, L., Muller, E. I., Silva Garcia, W. J. da, ... & Rhoden, C. R. B. (2023). Efficient Uptake of Angiotensin-Converting Enzyme II Inhibitor Employing Graphene Oxide-Based Magnetic Nanoadsorbents. *Water*, *15*(2), Article 2. Recovered from: https://doi.org/10.3390/w15020293

Ouaddari, H., Abbou, B., Lebkiri, I., Habsaoui, A., Ouzzine, M., & Fath Allah, R. (2024). Removal of Methylene Blue by adsorption onto natural and purified clays: Kinetic and thermodynamic study. *Chemical Physics Impact*, *8*, 100405. Recovered from: https://doi.org/10.1016/j.chphi.2023.100405

Pakizeh, M., Moradi, A., & Ghassemi, T. (2021). Chemical extraction and modification of chitin and chitosan from shrimp shells. *European Polymer Journal*, *159*, 110709. Recovered from: https://doi.org/10.1016/j.eurpolymj.2021.110709

Rashid, T. U., Kabir, S. M. F., Biswas, M. C., & Bhuiyan, M. A. R. (2020). Sustainable Wastewater Treatment via Dye–Surfactant Interaction: A Critical Review. *Industrial & Engineering Chemistry Research*, *59*(21), 9719–9745. Recovered from: https://doi.org/10.1021/acs.iecr.0c00676

Rekik, S. B., Gassara, S., Bouaziz, J., Deratani, A., & Baklouti, S. (2017). Development and characterization of porous membranes based on kaolin/chitosan composite. *Applied Clay Science*, *143*, 1–9. Recovered from: https://doi.org/10.1016/j.clay.2017.03.008

Rezende, M. J. C., Pereira, M. S. C., Santos, G. F. N., Aroeira, G. O. P., Albuquerque Jr., T. C., Suarez, P. A. Z., & Pinto, A. C. (2012). Preparation, characterisation and evaluation of brazilian clay-based catalysts for use in esterification reactions. *Journal of the Brazilian Chemical Society*, *23*, 1209–1215. Recovered from: https://doi.org/10.1590/S0103-50532012000700003

Ribeiro, G. A. C., Silva, D. S. A., Santos, C. C. dos, Vieira, A. P., Bezerra, C. W. B., Tanaka, A. A., & Santana, S. A. A. (2017). Removal of Remazol brilliant violet textile dye by adsorption using rice hulls. *Polímeros*, *27*, 16–26. Recovered from: https://doi.org/10.1590/0104-1428.2386

Rocha, F. N., Suarez, P. A. Z., & Guimarães, E. M. (2014). Clays and their Applications in Pottery and Ceramics Materials. *Revista Virtual de Química*, *6*(4). Recovered from: https://doi.org/10.5935/1984-6835.20140070

Saba, B., Kjellerup, B. V., & Christy, A. D. (2021). Eco-friendly bio-electro-degradation of textile dyes wastewater. *Bioresource Technology Reports*, *15*, 100734. Recovered from: https://doi.org/10.1016/j.biteb.2021.100734

Santos, B. F. dos, Maciel, A. M., Tavares, A. A., Araújo Fernandes, C. Q. B. de, Sousa, W. J. B. de, Lia Fook, M. V., Farias Leite, I., & Lima Silva, S. M. de. (2018). Synthesis and Preparation of Chitosan/Clay Microspheres: Effect of Process Parameters and Clay Type. *Materials*, *11*(12), Article 12. Recovered from: https://doi.org/10.3390/ma11122523

Shen, J., Huang, G., An, C., Xin, X., Huang, C., & Rosendahl, S. (2018). Removal of Tetrabromobisphenol A by adsorption on pinecone-derived activated charcoals: Synchrotron FTIR, kinetics and surface functionality analyses. *Bioresource Technology*, *247*, 812–820. Recovered from: https://doi.org/10.1016/j.biortech.2017.09.177

Silva, A. O., Cunha, R. S., Hotza, D., & Machado, R. A. F. (2021). Chitosan as a matrix of nanocomposites: A review on nanostructures, processes, properties, and applications. *Carbohydrate Polymers*, *272*, 118472. Recovered from: https://doi.org/10.1016/j.carbpol.2021.118472

Singh, R., Munya, V., Are, V. N., Nayak, D., & Chattopadhyay, S. (2021). A Biocompatible, pH-Sensitive, and Magnetically Separable Superparamagnetic Hydrogel Nanocomposite as an Efficient Platform for the Removal of Cationic Dyes in Wastewater Treatment. *ACS Omega*, *6*(36), 23139–23154. Recovered from: https://doi.org/10.1021/acsomega.1c02720

Singhapong, W., Jaroenworaluck, A., & Manpetch, P. (2024). Novel and Reusable Graphene Oxide-Coated Reticulated Open-Cell Mullite Foams for Methylene Blue Dye Adsorption. *ACS Omega*, *9*(5), 5541–5547. Recovered from: https://doi.org/10.1021/acsomega.3c07569

Sips, R. (1948). On the Structure of a Catalyst Surface. *The Journal of Chemical Physics*, *16*(5), 490–495. Recovered from: https://doi.org/10.1063/1.1746922

Sirajudheen, P., Poovathumkuzhi, N. C., Vigneshwaran, S., Chelaveettil, B. M., & Meenakshi, S. (2021). Applications of chitin and chitosan based biomaterials for the adsorptive removal of textile dyes from water—A comprehensive review. *Carbohydrate Polymers*, *273*, 118604. Recovered from: https://doi.org/10.1016/j.carbpol.2021.118604

Staroszczyk, H., Sztuka, K., Wolska, J., Wojtasz-Pająk, A., & Kołodziejska, I. (2014). Interactions of fish gelatin and chitosan in uncrosslinked and crosslinked with EDC films: FT-IR study. *Spectrochimica Acta Part A: Molecular and Biomolecular Spectroscopy*, *117*, 707–712. Recovered from: https://doi.org/10.1016/j.saa.2013.09.044

Salles, T. da R., Schnorr, C., Bruckmann, F. da S., Vicensi, E. C., Viana, A. R., Schuch, A. P., Garcia W. de J. da S., ... & Rhoden, C. R. B. (2023). Effective diuretic drug uptake employing magnetic carbon nanotubes derivatives: Adsorption study and in vitro geno-cytotoxic assessment. *Separation and Purification Technology*, *315*, 123713. Recovered from: https://doi.org/10.1016/j.seppur.2023.123713

Topcu, C., Caglar, B., Onder, A., Coldur, F., Caglar, S., Guner, E. K., Cubuk, O., & Tabak, A. (2018). Structural characterization of chitosan-smectite nanocomposite and its application in the development of a novel potentiometric monohydrogen phosphate-selective sensor. *Materials Research Bulletin*, *98*, 288–299. Recovered from: https://doi.org/10.1016/j.materresbull.2017.09.068

Tran, N. N., Escribà-Gelonch, M., Sarafraz, M. M., Pho, Q. H., Sagadevan, S., & Hessel, V. (2023). Process Technology and Sustainability Assessment of Wastewater Treatment. *Industrial & Engineering Chemistry Research*, *62*(3), 1195–1214. Recovered from: https://doi.org/10.1021/acs.iecr.2c03471

Vasconcelos, M. W., Gonçalves, S., Oliveira, E. C. de, Rubert, S., & Ghisi, N. de C. (2022). Textile effluent toxicity trend: A scientometric review. *Journal of Cleaner Production*, *366*, 132756. Recovered from: https://doi.org/10.1016/j.jclepro.2022.132756

Vithalkar, S. H., & Jugade, R. M. (2020). Adsorptive removal of crystal violet from aqueous solution by cross-linked chitosan coated bentonite. *Materials Today: Proceedings*, *29*, 1025–1032. Recovered from: https://doi.org/10.1016/j.matpr.2020.04.705

Wade C. Driscoll. (1996). Robustness of the ANOVA and Tukey-Kramer statistical tests. *Computers & Industrial Engineering*, *31*(1–2), 265–268. Recovered from: https://doi.org/10.1016/0360-8352(96)00127-1

Zhao, T., Xu, S., & Hao, F. (2023). Differential adsorption of clay minerals: Implications for organic matter enrichment. *Earth-Science Reviews*, *246*, 104598. Recovered from: https://doi.org/10.1016/j.earscirev.2023.104598

Zhou, Q., Gao, Q., Luo, W., Yan, C., Ji, Z., & Duan, P. (2015). One-step synthesis of amino-functionalized attapulgite clay nanoparticles adsorbent by hydrothermal carbonization of chitosan for removal of methylene blue from wastewater. *Colloids and Surfaces A: Physicochemical and Engineering Aspects*, *470*, 248–257. Recovered from: https://doi.org/10.1016/j.colsurfa.2015.01.092

Zouaoui, F., Bourouina-Bacha, S., Bourouina, M., Jaffrezic-Renault, N., Zine, N., & Errachid, A. (2020). Electrochemical sensors based on molecularly imprinted chitosan: A review. *TrAC Trends in Analytical Chemistry*, *130*, 115982. Recovered from: https://doi.org/10.1016/j.trac.2020.115982

Authorship contributions

1 – Mateus Veras Pereira

PhD student in Chemistry at UNICAMP, Master's degree in Chemistry at UNICAMP
https://orcid.org/0000-0002-7119-0249 • m265987@dac.unicamp.br
Contribution: Conceptualization, Data curation, Investigation, Formal analysis, Methodology, Validation, Visualization, Writing – original draft.

2 – Mauro Cosme de Carvalho Goes

Researcher in the Chemistry of Interfaces and Materials laboratory at UFMA, PhD in Biodiversity and Biotechnology at UFMA
https://orcid.org/0000-0001-7056-8353 • maurocosme@gmail.com
Contribution: Data curation, Visualization, Writing – review & editing

3 – Rodolfo Araújo Fernandes

Master student in Chemistry at UFMA, Degree in Chemistry at UEMA
https://orcid.org/0009-0008-1103-988X • qmcrodolfo@gmail.com
Contribution: Writing – review & editing

4 – Suzyeth Monteiro Melo

Chemist at UFMA in the Department of Oceanography and Limnology (DEOLI), PhD in Analytical and Inorganic Chemistry at IQSC - USP
https://orcid.org/0009-0006-9928-9941 • sm.melo@ufma.br
Contribution: Writing – review & editing

5 – Joacy Batista de Lima

Full Professor at the Department of Chemistry at UFMA; PhD in Chemistry at IQSC - USP https://orcid.org/0000-0002-1826-2768 • joacy.lima@ufma.br
Contribution: Writing – review & editing

6 – Cicero Wellington Brito Bezerra

Full Professor at the Department of Chemistry at UFMA; PhD in Chemistry at IQSC - USP
https://orcid.org/0000-0001-9058-9469 • cwb.bezerra@ufma.br
Contribution: Conceptualization, Methodology, Project administration, Resources, Validation, Visualization, Writing – review & editing, Supervision, Funding acquisition.

How to quote this article

Pereira, M. V.; Goes, M. C. de C.; Fernandes, R. A.; Melo, S. M.; Lima, J. B. de & Bezerra, C. W. B. (2025). Chitosan/smectite spheres for methylene blue removal: preparation and characterization. *Ciencia e Natura*, 47, e86389. doi: 10.5902/2179460X86389.